Locally self-similar formulation for hypersonic laminar boundary layers in thermochemical nonequilibrium

By C. Williams, M. Di Renzo†, P. Moin AND J. Urzay

1. Motivation and objectives

The consideration of finite-rate thermochemical effects induced by high temperatures, including vibrational and chemical relaxation, complicates significantly the description of flows around bodies moving hypersonically. The inviscid flow in the shock layer is influenced by the shock-front curvature induced by the thermochemical relaxation in the post-shock gas (Sharma & Shyam 1984; Anderson 2006). This shock-front curvature is present in addition to that induced by finite leading-edge bluntness, as schematically indicated in Figure 1(a). Its origin is related to the isobaric increase in density associated with thermochemical relaxation, as schematically shown in the cross-section profiles in Figure 1(b). This increase in density induces a gradient of the normal component of the post-shock velocity in the direction normal to the shock that can only be accommodated if the shock front is curved. Since the transverse entropy gradient produced by the shock-front curvature leads to vorticity in the post-shock gas, the boundary layer sees boundary conditions away from the wall that are characterized by a vortical inviscid flow in the shock layer that is subject to a favorable streamwise pressure gradient induced by the thermochemical relaxation, as indicated in Figure 1(c). This is in contrast to the supersonic flow of thermochemically frozen (i.e., calorically perfect) gases over sharp-nose bodies, where a clear separation exists between the boundary and shock layers, such that one can integrate the inner viscous problem using the overriding, uniform inviscid flow as a well-defined boundary condition at infinity.

Complexities similar to those discussed above, albeit focused on the effect that entropy layers induced by blunt edges have on post-shock laminar boundary layers, were identified early by Ferri & Libby (1954). To facilitate the integration of the problem with rotational inviscid-flow conditions outside the boundary layer, which are responsible for significant variations in skin friction and wall heating relative to the irrotational case, subsequent theories found it necessary to retain second-order terms in the perturbation expansion, leading to modified laminar boundary-layer equations (Davis & Flügge-Lotz 1964; Van Dyke 1969). Thermochemical-nonequilibrium aspects of the problem have been much less explored, with a notable analysis being made by Seror *et al.* (1997) using an alternative, defect-boundary-layer method.

Our first pass at this problem is much more modest than the approaches identified above. Using a two-temperature description, this report focuses on extending the locally self-similar formulation of Lees (1956) [see also Fay & Riddell (1958) and Liñán & Da Riva (1962)] for compressible laminar boundary layers in order to include thermochemical-nonequilibrium effects, namely vibrational and chemical relaxation, as well as the coupling between these processes. These effects are incorporated both in the inner viscous

† CERFACS, France

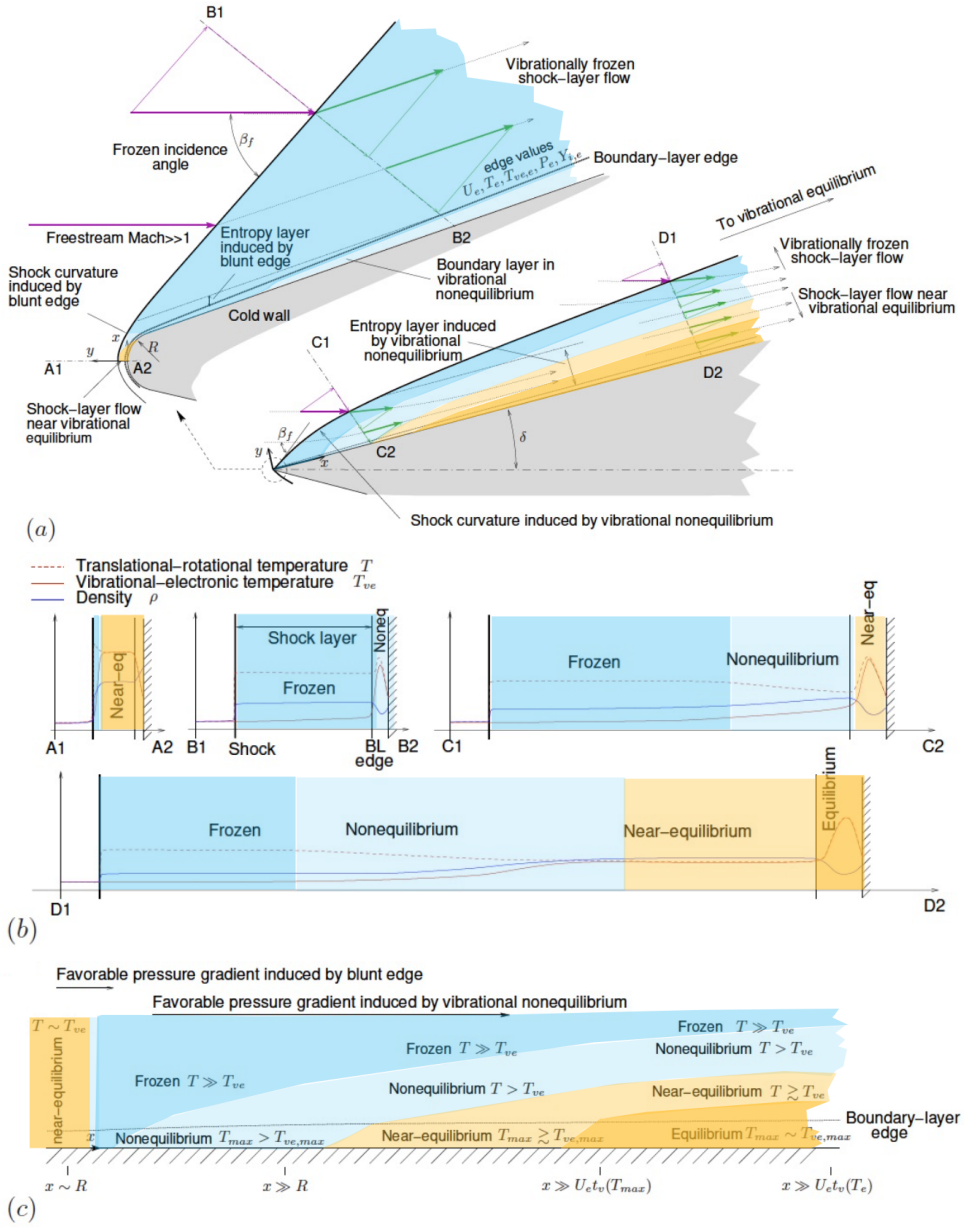

FIGURE 1. Schematics of a hypersonic flow over a two-dimensional wedge highlighting vibrational-nonequilibrium phenomena, including (a) large-scale and zoomed views of the shock layer, (b) temperature and density profiles along the cross sections A1-A2, B1-B2, C1-C2, and D1-D2 indicated in the top panel, and (c) flow near the surface. Addition of chemical effects to these schematics would require extra relaxation time scales and extra shock-front curvature.

region and in the outer inviscid flow. However, the latter is assumed to be irrotational. As deduced from the considerations above, this formulation is of practical relevance only when the gas in the inviscid shock layer is either (a) vibrationally frozen, (b) in vibrational equilibrium but chemically frozen, or (c) in both vibrational and chemical

equilibrium. In these three cases, the resulting shock-front curvature is zero, there is no thermochemistry-driven entropy layer, and the inviscid flow in the shock layer overriding the boundary layer becomes irrotational, thereby rendering a well-defined boundary condition at infinity that does not require consideration of higher-order boundary-layer effects. However, thermochemical nonequilibrium can still arise within the boundary layer due to the large temperature gradients caused by viscous aerodynamic heating.

These approximations limit the scope of the present study, but also hint at interesting fundamental work that remains to be done to describe the coupling between thermochemistry-driven entropy layers and hypersonic laminar boundary layers. Much less is known about this interaction in transitional and turbulent boundary layers, but this is a different question that will be left for future research.

The remainder of this report is organized as follows. The formulation of the problem is summarized in Section 2. A numerical solution is discussed in Section 3. Lastly, conclusions are given in Section 4.

2. Formulation

This section begins by outlining the two-dimensional boundary-layer conservation equations in a two-temperature framework, followed by their transformed versions after defining a self-similar pair of coordinates. Unless otherwise specified, all notation and models employed in this report follow those provided in Di Renzo *et al.* (2020) and Williams *et al.* (2021) in this volume, and therefore the details will be spared and the mathematical symbols will not be redefined here.

2.1. *Two-dimensional boundary-layer conservation equations*

Consider the two-dimensional boundary-layer conservation equations of mass, momentum, species, stagnation enthalpy, and vibrational-electronic internal energy, namely

$$\frac{\partial}{\partial x}(\rho u) + \frac{\partial}{\partial y}(\rho v) = 0, \tag{2.1}$$

$$\rho u\frac{\partial u}{\partial x} + \rho v\frac{\partial u}{\partial y} = -\frac{dP_e}{dx} + \frac{\partial}{\partial y}\left(\mu\frac{\partial u}{\partial y}\right), \tag{2.2}$$

$$\rho u\frac{\partial Y_i}{\partial x} + \rho v\frac{\partial Y_i}{\partial y} = -\frac{\partial}{\partial y}\left(\rho Y_i V_{yi}\right) + \dot{w}_i, \tag{2.3}$$

$$\rho u\frac{\partial h_0}{\partial x} + \rho v\frac{\partial h_0}{\partial y} = \frac{\partial}{\partial y}\left(\mu\frac{\partial u}{\partial y} + \lambda_{tr}\frac{\partial T}{\partial y} + \lambda_{ve}\frac{\partial T_{ve}}{\partial y} - \sum_{i=1}^{N_s}\rho Y_i V_{yi} h_i\right), \tag{2.4}$$

and

$$\rho u\frac{\partial e_{ve}}{\partial x} + \rho v\frac{\partial e_{ve}}{\partial y} = \frac{\partial}{\partial y}\left(\lambda_{ve}\frac{\partial T_{ve}}{\partial y} - \sum_{i=1}^{N_s}\rho Y_i V_{yi} e_{ve,i}\right) + \sum_{i=1}^{N_s}\rho Y_i\frac{(e^*_{v,i} - e_{v,i})}{\tau_i} + \dot{w}_{ve}, \tag{2.5}$$

where

$$V_{yi} = -\frac{D_i}{X_i}\frac{\partial X_i}{\partial y} + \sum_{i=1}^{N_s} Y_i\frac{D_i}{X_i}\frac{\partial X_i}{\partial y} \tag{2.6}$$

is the wall-normal component of the diffusion velocity of species i, with $i = 1, 2, \ldots N_s$. In this approximation, the thermodynamic pressure is assumed to be constant through the

boundary layer and equal to the edge pressure P_e, which is related to the local density, species concentration, and translational-rotational temperature as

$$P_e = \rho \mathrm{R}^0 T / \overline{\mathcal{M}}. \tag{2.7}$$

Equations (2.1-2.5) are subject to the edge values

$$\rho = \rho_e, \quad u = U_e, \quad Y_i = Y_{i,e}, \quad T = T_e, \quad \text{and} \quad T_{ve} = T_{ve,e} \tag{2.8}$$

away from the wall in the inviscid shock layer at $y \to \infty$, and to

$$u = v = 0, \quad \partial Y_i / \partial y = 0, \quad \text{and} \quad T = T_{ve} = T_w \tag{2.9}$$

at the wall $y = 0$, where T_w is the wall temperature. In this study, the edge values of density, velocity, mass fractions, translational-rotational temperature, and vibrational-electronic temperature in the boundary conditions (2.8) are assumed to be constant with the streamwise distance x.

2.2. *Locally self-similar boundary-layer conservation equations*

Consider the similarity variables (Lees 1956)

$$\xi(x) = \rho_e \mu_e U_e x \quad \text{and} \quad \eta(x,y) = \frac{U_e}{\sqrt{2\xi}} \int_0^y \rho dy, \tag{2.10}$$

where μ_e is the edge dynamic viscosity. A streamfunction $\psi = f(\eta)\sqrt{2\xi}$ can be defined to automatically satisfy the continuity equation (2.1), in such a way that $u = U_e f'$ and $\rho v = -\rho_e \mu_e U_e f / \sqrt{2\xi} - \eta_x f' \sqrt{2\xi}$, where primes indicate differentiation with respect to η, and $\eta_x = \partial \eta / \partial x$ is a metric coefficient. In these variables, the momentum conservation equation (2.2) becomes

$$(C f'')' + f f'' = 0, \tag{2.11}$$

where $C = \rho\mu / (\rho_e \mu_e)$ is the Chapman-Rubesin parameter. Similarly, the species conservation equation (2.3) becomes

$$\left[\frac{C_i Y_i}{Sc_{i,e}} \left(\frac{X_i'}{X_i} - \sum_{j=1}^{N_s} \frac{D_j Y_j}{D_i X_j} X_j' \right) \right]' + f Y_i' + 2 Da_{c,i} \dot{\mathcal{W}}_i = 0 \tag{2.12}$$

for $i = 1, 2 \ldots, N_s$, where $C_i = \rho^2 D_i / \left(\rho_e^2 D_{i,e}\right)$ is a dimensionless group of variables similar to the Chapman-Rubesin parameter but for species transport, and $Sc_{i,e} = \mu_e / (\rho_e D_{i,e})$ is a Schmidt number based on the edge diffusion coefficient $D_{i,e}$. In addition, $Da_{c,i} = x / (U_e t_{c,i})$ is a chemical Damköhler number defined as the ratio of the residence time x/U_e to the characteristic chemical time $t_{c,i}$ based on the edge translational-rotational temperature T_e, with $t_{c,i}$ being also used for normalization of the chemical production rate as $\dot{\mathcal{W}}_i = t_{ch,i} \dot{w}_i / \rho$.

The transformed version of the stagnation enthalpy conservation equation (2.4) is

$$\begin{aligned} &\frac{c_{p,e}^{tr} T_e}{h_{0,e}} \left(\frac{C_{tr} \theta'}{Pr_{tr,e}} \right)' + \frac{c_{p,e}^{ve} T_{ve,e}}{h_{0,e}} \left(\frac{C_{ve} \theta_{ve}'}{Pr_{ve,e}} \right)' + f m' + \frac{U_e^2}{h_{0,e}} \left(C f' f'' \right)' \\ &\qquad + \sum_{i=1}^{N_s} \frac{h_{i,e}}{h_{0,e}} \left[\frac{C_i g_i Y_i}{Sc_{i,e}} \left(\frac{X_i'}{X_i} - \sum_{k=1}^{N_s} \frac{D_j Y_j}{D_i X_j} X_j' \right) \right]' = 0, \end{aligned} \tag{2.13}$$

where $\theta = T/T_e$ and $\theta_{ve} = T_{ve}/T_{ve,e}$ are the dimensionless translational-rotational and

vibrational-electronic temperatures, respectively. The quantities $C_{tr} = \rho\lambda_{tr}/(\rho_e\lambda_{tr,e})$ and $C_{ve} = \rho\lambda_{ve}/(\rho_e\lambda_{ve,e})$ are dimensionless groups of variables that give rise to the translational-rotational and vibrational-electronic Prandtl numbers, $Pr_{tr,e} = \mu_e c_{p,e}^{tr}/\lambda_{tr,e}$ and $Pr_{ve,e} = \mu_e c_{p,e}^{ve}/\lambda_{ve,e}$, respectively, which are based on the corresponding edge values of the thermal conductivities $\lambda_{tr,e}$ and $\lambda_{ve,e}$, and on the specific heats of the edge gas at constant pressure, $c_{p,e}^{tr}$ and $c_{p,e}^{ve}$. Additionally, $g_i = h_i/h_{i,e}$ is the specific partial enthalpy normalized with the corresponding edge value $h_{i,e}$. The symbol $m = h_0/h_{0,e}$ denotes the specific stagnation enthalpy divided by its edge value $h_{0,e}$. In particular, using the definition $h_0 = u^2/2 + \sum_{i=1}^{N_s} Y_i h_i$, the expression

$$m = \left(\frac{U_e^2}{2h_{0,e}}\right) f'^2 + \sum_{i=1}^{N_s} \left(\frac{h_{i,e}}{h_{0,e}}\right) Y_i g_i \tag{2.14}$$

is obtained that relates m, Y_i, and f. Furthermore, the dimensionless partial specific enthalpy g_i can be related to θ and θ_{ve} by conveniently normalizing Eq. (2.3) in Williams *et al.* (2021) as

$$g_i = g_{i,ref} + \frac{c_{p,e}^{tr} T_e}{h_{i,e}} \int_{\theta_{ref}}^{\theta} \frac{c_{p,i}^{tr}(\theta)}{c_{p,e}^{tr}} d\theta + \left(\frac{e_{ve,i,e}}{h_{i,e}}\right) \mathcal{E}_{ve,i}, \tag{2.15}$$

where $\mathcal{E}_{ve,i} = e_{ve,i}/e_{ve,i,e}$ is the dimensionless partial specific vibrational-electronic internal energy of species i. In particular, $\mathcal{E}_{ve,i}$ is a non-linear function of θ_{ve} obtained by normalizing the sum of Eqs. (2.5) and (2.6) in Williams *et al.* (2021) as

$$\mathcal{E}_{ve,i} = \frac{(\mathcal{V}\mathrm{R}^0\Theta_{v,i})/(\mathcal{M}_i e_{ve,i,e})}{\exp(\beta_{v,i}/\theta_{ve}) - 1} + \left(\frac{\mathrm{R}^0 T_{ve,e}}{\mathcal{M}_i e_{ve,i,e}}\right) \theta_{ve}^2 \frac{\partial}{\partial\theta_{ve}} \left\{ \ln \left[\sum_j g_{i,j} \exp(-\beta_{el,i,j}/\theta_{ve}) \right] \right\}. \tag{2.16}$$

where $\beta_{v,i} = \Theta_{v,i}/T_{ve}$ and $\beta_{el,i,j} = \Theta_{el,i,j}/T_{ve}$ are characteristic dimensionless temperatures of vibrational and electronic energy modes, and $\mathcal{V}$ is a prefactor equal to 0 and 1 for monoatomic and diatomic species, respectively.

To close the system of equations, the vibrational-electronic energy conservation equation (2.5) can be recast into

$$\begin{aligned} &\frac{c_{p,e}^{ve} T_e}{e_{ve,e}} \left(\frac{C_{ve}\theta'_{ve}}{Pr_{ve,e}}\right)' + f\mathcal{E}'_{ve} + \sum_{i=1}^{N_s} \frac{e_{ve,i,e}}{e_{ve,e}} \left[\frac{C_i \mathcal{E}_{ve,i} Y_i}{Sc_{e,i}} \left(\frac{X'_i}{X_i} - \sum_{k=1}^{N_s} \frac{D_j Y_j}{D_i X_j} X'_j \right) \right]' \\ &\quad + 2\sum_{i=1}^{N_s} Da_{v,i} Y_i \left(\frac{e_{v,i,e}}{e_{ve,e}}\right) \frac{(\mathcal{E}^*_{v,i} - \mathcal{E}_{v,i})}{\mathcal{T}_i} + 2\sum_{i=1}^{N_s} Da_{c,i} \dot{\mathcal{W}}_{ve,i} \left(\frac{e_{ve,i,e}}{e_{ve,e}}\right) = 0, \end{aligned} \tag{2.17}$$

where $\mathcal{E}_{ve} = e_{ve}/e_{ve,e}$ is the dimensionless vibrational-electronic specific internal energy, and $\mathcal{E}_{v,i} = e_{v,i}/e_{v,i,e}$ is the dimensionless partial specific vibrational internal energy corresponding to the first term on the right-hand side of Eq. (2.16), with $\mathcal{E}^*_{v,i}$ being its equilibrium value evaluated at the local translational-rotational temperature θ. Additionally, $\mathcal{T}_i = \tau_i/t_{v,i}$ is a dimensionless local vibrational-relaxation time based on the characteristic value $t_{v,i}$ obtained by evaluating Eq. (2.9) in Williams *et al.* (2021) at the edge translational-rotational temperature in the boundary layer. Premultiplying the Landau-Teller relaxation term is the vibrational Damköhler number $Da_{v,i} = x/(U_e t_{v,i})$, which is defined as the ratio of the residence time to the edge vibrational-relaxation time.

Lastly, $\dot{\mathcal{W}}_{ve,i}$ represents the chemical production rate of vibrational-electronic internal energy of species i normalized with $\rho e_{ve,i,e}/t_{c,i}$.

Note that both $Da_{v,i}$ and $Da_{c,i}$ have been arbitrarily chosen above to be defined in terms of edge conditions. This is obviously not the best scaling for these two parameters when the wall is cold relative to the edge stagnation temperature, in that much larger temperatures can develop in the boundary layer because of viscous aerodynamic heating. As a result, the effective Damköhler numbers can be much larger than the values predicted by using edge reference values, thereby rendering thermochemical nonequilibrium in the boundary layer while the outer inviscid flow is thermochemically frozen. This situation is reminiscent of that observed in non-premixed combustion, where a correct scaling of the chemical time requires estimation of local conditions in the hot reacting zone. The formulation above can therefore be modified to incorporate these considerations by rescaling the vibrational and chemical relaxation times based on conditions near the temperature peak in the boundary layer.

These equations need to be supplemented with the transformed version of the ideal-gas equation of state (2.7), namely

$$\mathcal{R}\theta\overline{\mathcal{M}}_e/\overline{\mathcal{M}} = 1, \tag{2.18}$$

where $\mathcal{R} = \rho/\rho_e$ is the dimensionless density, and $\overline{\mathcal{M}}_e$ is the molecular weight of the mixture at the boundary-layer edge. The boundary conditions are

$$f' = 1, \quad Y_i = Y_{i,e}, \quad \text{and} \quad \theta = \theta_{ve} = 1 \tag{2.19}$$

away from the wall in the inviscid shock layer at $\eta \to \infty$, along with

$$f = f' = 0, \quad Y_i' = 0, \quad \theta = T_w/T_e, \quad \text{and} \quad \theta_{ve} = T_w/T_{ve,e} \tag{2.20}$$

at the wall $\eta = 0$.

The formulation provided above represents a locally self-similar boundary-value problem, in that, for a given value of x, the problem can be integrated to yield a solution that is only a function of the self-similar coordinate η. The incorporation of finite-rate thermochemistry in the problem necessarily implies an evolution of the solution with x in a manner that depends on externally imposed time scales of chemical and vibrational relaxation, which rules out complete self-similarity (Liñán & Da Riva 1962).

3. Numerical solution

The system of ordinary differential equations (2.11), (2.12), (2.13), and (2.17), subject to the boundary conditions (2.19) and (2.20), and supplemented with Eqs. (2.14), (2.15) and (2.16), are solved numerically in this section using a second-order finite-difference discretization and a Newton-Raphson solver with a line-search algorithm.

3.1. *Particular aspects of the thermochemical models*

The formulation presented in Section 2 is independent of particular closure models for the chemical production rates of species, $\dot{w}_i$, and vibrational-electronic internal energy, $\dot{w}_{ve}$. In this section, use of the models of Marrone & Treanor (1963) [referred to as CVDV model below] and Park (1990) is made to calculate $\dot{w}_i$ and $\dot{w}_{ve}$. Specifically, in the approach of Park followed here, the dissociation rates are evaluated at the geometric mean temperature $\sqrt{\theta\theta_{ve}}$, and the calculation of $\dot{w}_{ve}$ is made using either the preferential dissociation model of Sharma *et al.* (1992) [referred to as Park-P model below], or the non-preferential one of Candler & MacCormack (1991) [referred to as Park-NP model below].

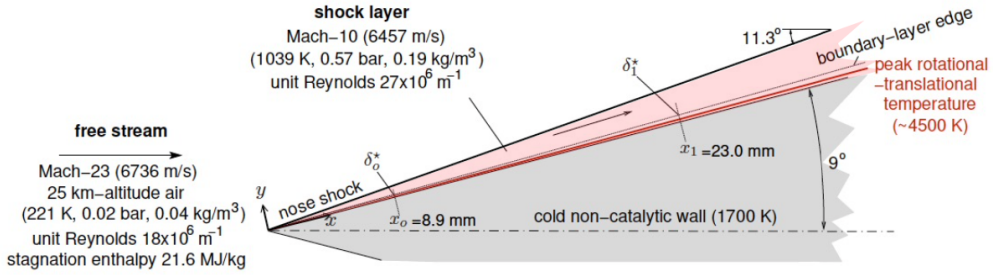

FIGURE 2. Schematics of the configuration.

The solutions obtained using Park's and CVDV models are compared with those obtained in the infinitely-fast vibrational-relaxation limit corresponding to a single-temperature description [referred to as thermal-equilibrium (TE) solution below].

A standard five-step dissociation mechanism for high-temperature air is considered that includes N_2, O_2, NO, N, and O (Park 1990). Thermophysical and transport properties used in these calculations are discussed in Di Renzo *et al.* (2020) and Williams *et al.* (2021). The reader is referred to the seminal treatise of Park (1990) for details on two-temperature descriptions of hypersonic flows.

3.2. *Results*

The case analyzed here is represented in Figure 2 and corresponds to the same free-stream conditions and geometry used in Di Renzo & Urzay (2021), in which an infinitely sharp, planar wedge of semiangle 9° moves at Mach 23 in air at 25 km of altitude. This case is particularly amenable to this formulation because of the following reasons. The resulting post-shock temperature is relatively low, $T_e = 1039$ K, which leaves air mostly undissociated in the shock layer, with resulting edge mass fractions $Y_{\mathrm{N}_2,e} = 0.767$ and $Y_{\mathrm{O}_2,e} = 0.233$. At these conditions, the vibrational energy of the post-shock gas represents approximately less than 6% of the internal energy. As a result, the vibrational energy is in equilibrium near its ground level, $e_{v,\mathrm{N}_2,e} \simeq e^*_{v,\mathrm{N}_2,e}$ and $e_{v,\mathrm{O}_2,e} \simeq e^*_{v,\mathrm{O}_2,e}$. However, the characteristic vibrational-relaxation times t_{v,N_2} and t_{v,O_2} are exceedingly large at this post-shock temperature. The post-shock gas is therefore undergoing a very slow, low-temperature vibrational relaxation at vanishing vibrational energy. From the viewpoint of the Landau-Teller relaxation term in Eq. (2.17), this combination of events in the post-shock gas renders vanishing vibrational Damköhler numbers, $Da_{v,i} \to 0$, and a vanishing vibrational-energy slip at the boundary-layer edge, $\mathcal{E}_{v,\mathrm{N}_2,e} \simeq \mathcal{E}^*_{v,\mathrm{N}_2,e}$ and $\mathcal{E}_{v,\mathrm{O}_2,e} \simeq \mathcal{E}^*_{v,\mathrm{O}_2,e}$. The resulting regime resembles the one discussed at the bottom of page 253 of Vincenti & Kruger (1965), which corresponds to an inviscid post-shock flow that is at the same time both vibrationally frozen and in vibrational equilibrium. Consequently, it does not make any significant difference for the dynamics to consider the gas in one state versus the other. In both cases, the shock-front curvature vanishes and the inviscid flow in the shock layer is irrotational.

Based on the considerations above, the simplest approach of taking the two temperatures equal at the edge of the boundary layer, $T = T_{ve} = T_e$, is followed here. The remaining edge conditions are provided in Figure 2. The wall is assumed to be isothermal at temperature $T_w = 1700$ K corresponding to approximately 10% of the edge

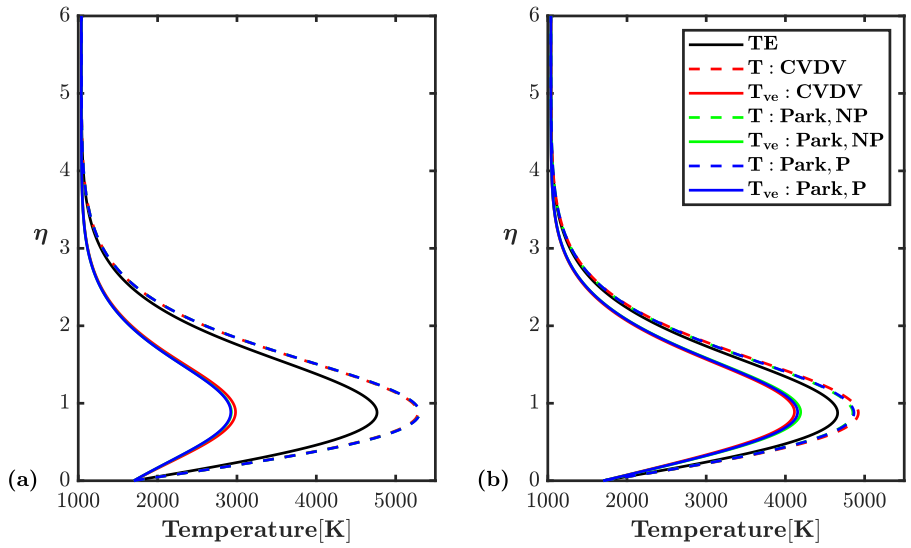

FIGURE 3. Temperature profiles at two streamwise stages along the wedge surface: (a) $x_o = 8.9$ mm (corresponding to $Da_{v,\mathrm{O}_2} = 0.007$ and $Re_x = 250,000$) and (b) $x_1 = 23.0$ mm (corresponding to $Da_{v,\mathrm{O}_2} = 0.018$ and $Re_x = 650,000$). The Park-P and Park-NP models yield indistinguishable results in panel (a).

stagnation temperature, which warrants the presence of a temperature maximum within the boundary layer and a heat flux directed toward the surface, as shown in Figure 3.

The higher temperatures engendered in the boundary layer by viscous aerodynamic heating result in order-unity values of the local vibrational Damköhler number for O_2, thereby leading to significant vibrational nonequilibrium there. As expected from the correspondingly larger residence time, the extent of vibrational nonequilibrium decays with increasing streamwise distance (or equivalently, with increasing vibrational and chemical Damköhler numbers, and with increasing Reynolds number $Re_x = \rho_e U_e x/\mu_e$).

Whereas the non-preferential Park model predicts the most rapid equilibration of the vibrational-electronic temperature, the CVDV model yields a comparatively lower vibrational-electronic temperature, consistent with its assumption that the vibrationally-excited molecules dissociate preferentially. However, the solutions obtained using the preferential Park model and the CVDV model are quite similar.

Figure 3 shows that the single-temperature profile obtained using vibrational equilibrium is everywhere intermediate to the translational-rotational and vibrational-electronic temperatures. However, the geometric mean temperature $\sqrt{TT_{ve}}$ is everywhere smaller than the single temperature obtained using vibrational equilibrium. As shown in Figure 4, this leads to smaller concentrations of air dissociation products when thermochemical nonequilibrium is incorporated via the approach of Park, since its dissociation rate constants are evaluated at the geometric mean temperature. Owing to its faster effective relaxation, the non-preferential Park model predicts slightly larger concentration of air dissociation products than its preferential counterpart. The concentration of air dissociation products decreases further with respect to the vibrational-equilibrium solution when the CVDV model is used.

It is worth mentioning that integral quantities such as the displacement thickness $\delta^\star$ (and consequently the displacement Reynolds number $Re_{\delta^\star} = \rho_e U_e \delta^\star/\mu_e$) are modified

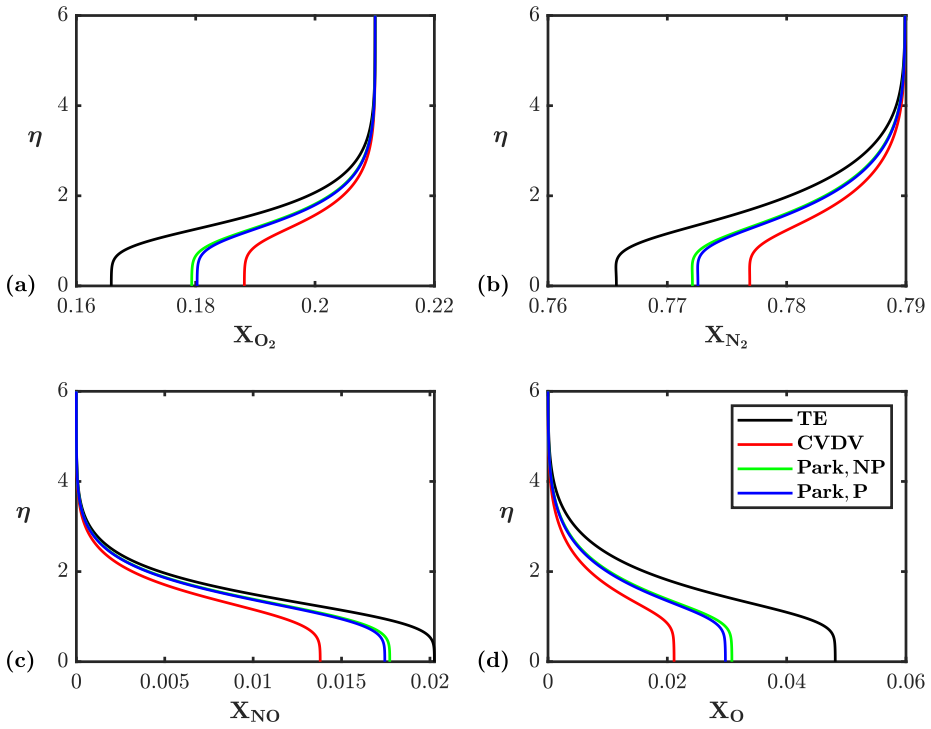

FIGURE 4. Molar-fraction profiles at $x_1 = 23.0$ mm for (a) O_2, (b) N_2, (c) NO and (d) O (corresponding to $Re_x = 650,000$ and $Da_{v,O_2} = 0.018$).

by the incorporation of vibrational nonequilibrium. For instance, at $x = x_o = 8.9$ mm, the vibrational-equilibrium solution gives $\delta_o^\star = 0.176$ mm and $Re_{\delta_o^\star} = 4968$, whereas the CVDV model gives $\delta_o^\star = 0.192$ mm and $Re_{\delta_o^\star} = 5436$. Similarly, at $x = x_1 = 23.0$ mm, the vibrational-equilibrium solution yields $\delta_1^\star = 0.281$ mm and $Re_{\delta_1^\star} = 7928$, whereas the CVDV model renders $\delta_1^\star = 0.293$ mm and $Re_{\delta_1^\star} = 8285$. These results suggests that, at equal distances from the wedge vertex, the boundary layer is thicker and has a higher Reynolds number when vibrational non-equilibrium is included because of comparatively smaller densities caused by the higher translational-rotational temperatures.

4. Conclusions

In this report, a locally self-similar formulation for hypersonic laminar boundary layers has been derived that incorporates thermochemical effects, namely vibrational and chemical relaxation, as well as their coupling. The formulation is integrated for the boundary layer around a 9-degree wedge moving at Mach 23 in air at 25 km of altitude. For this case, there are no significant differences in the temperature profiles obtained from three standard dissociation/vibrational-relaxation coupling models. A chief effect of vibrational nonequilibrium is to inhibit dissociation chemistry in the boundary layer, with the impact being most significant for molecular oxygen. The model of Marrone & Treanor (1963) predicts consistently lower concentrations of air dissociation products compared to approaches based on Park (1990). This formulation may be of some interest for imposing inflow boundary conditions in direct numerical simulations of hypersonic boundary layers (Franko & Lele 2013; Di Renzo & Urzay 2021).

Acknowledgments

This investigation was funded by the Advanced Simulation and Computing (ASC) program of the US Department of Energy's National Nuclear Security Administration (NNSA) via the PSAAP-III Center at Stanford, Grant No. DE-NA0002373. C.W. was funded by a Stanford School of Engineering Graduate Fellowship.

REFERENCES

Anderson, J. D. J. 2006 *Hypersonic and High-Temperature Gas Dynamics*. American Institute of Aeronautics and Astronautics.

Candler, G. V. & MacCormack, R. W. 1991 Computation of weakly ionized hypersonic flows in thermochemical nonequilibrium. *J. Thermophys. Heat Trans.* **5**, 266–273.

Davis, R.T. & Flügge-Lotz, I. 1964 Second-order boundary-layer effects in hypersonic flow past axisymmetric blunt bodies. *J. Fluid Mech.* **20**, 593–623.

Di Renzo, M., Fu, L. & Urzay, J. 2020 HTR solver: An open-source exascale-oriented task-based multi-GPU high-order code for hypersonic aerothermodynamics. *Comput. Phys. Comm.* **255**, 107262.

Di Renzo, M. & Urzay, J. 2021 Direct numerical simulation of a hypersonic transitional boundary layer at suborbital enthalpies. *J. Fluid Mech.* **912**, A29.

Fay, J. A. & Riddell, F. R. 1958 Theory of stagnation point heat transfer in dissociated air. *J. Aerosp. Sci.* **25**, 73–85.

Ferri, A. & Libby, P.A. 1954 Note on an interaction between the boundary layer and the inviscid flow. *J. Aeronaut. Sci.* **21**, 130–130.

Franko, K. J. & Lele, S. K. 2013 Breakdown mechanisms and heat transfer overshoot in hypersonic zero pressure gradient boundary layers. *J. Fluid Mech.* **730**, 491–532.

Lees, L. 1956 Laminar heat transfer over blunt-nosed bodies at hypersonic flight speeds. *J. Jet Propul.* **26**, 259–269.

Liñán, A. & Da Riva, I. 1962 Chemical nonequilibrium effects in hypersonic aerodynamics. DTIC TR # AD0294638.

Marrone, P. V. & Treanor, C. E. 1963 Chemical relaxation with preferential dissociation from excited vibrational levels. *Phys. Fluids* **6**, 1215–1221.

Park, C. 1990 *Nonequilibrium Hypersonic Aerothermodynamics*. Wiley.

Seror, S., Zeitoun, D.E., Brazier, J.P. & Schall, E. 1997 Asymptotic defect boundary layer theory applied to thermochemical non-equilibrium hypersonic flows. *J. Fluid Mech.* **339**, 213–238.

Sharma, V. D. & Shyam, R. 1984 On flows with vibrational relaxation behind an attached shock wave. *Acta Astronaut.* **11**, 91–101.

Sharma, S. P., Huo, W. M. & Park, C. 1992 Rate parameters for coupled vibration-dissociation in a generalized ssh approximation. *J. Thermophys. Heat Trans.* **6**, 9–21.

Van Dyke, M. 1969 Higher-order boundary-layer theory. *Annu. Rev. Fluid Mech.* **11**, 265–292.

Vincenti, W. G. & Kruger C. H. 1965 *Introduction to Physical Gas Dynamics*. Wiley.

Williams, C., Di Renzo, M. & Urzay, J. 2021 Two-temperature extension of the HTR solver for hypersonic turbulent flows in thermochemical nonequilibrium. *Annual Research Briefs,* Center for Turbulence Research, Stanford University, pp. 95-107.